# High-Fidelity Scientific Simulation Surrogates via Adaptive Implicit Neural Representations

Ziwei Li, Yuhan Duan, Tianyu Xiong, Yi-Tang Chen, Wei-Lun Chao, Han-Wei Shen

Department of Computer Science and Engineering
The Ohio State University
{li.5326, duan.418, xiong.336, chen.10522, chao.209, shen.94}@osu.edu

## **Abstract**

Effective surrogate models are critical for accelerating scientific simulations. Implicit neural representations (INRs) offer a compact and continuous framework for modeling spatially structured data, but they often struggle with complex scientific fields exhibiting localized, high-frequency variations. Recent approaches address this by introducing additional features along rigid geometric structures (e.g., grids), but at the cost of flexibility and increased model size. In this paper, we propose a simple yet effective alternative: Feature-Adaptive INR (FA-INR). FA-INR leverages cross-attention to an augmented memory bank to learn flexible feature representations, enabling adaptive allocation of model capacity based on data characteristics, rather than rigid structural assumptions. To further improve scalability, we introduce a coordinate-guided mixture of experts (MoE) that enhances the specialization and efficiency of feature representations. Experiments on three large-scale ensemble simulation datasets show that FA-INR achieves state-of-the-art fidelity while significantly reducing model size, establishing a new trade-off frontier between accuracy and compactness for INR-based surrogates.

## 1 Introduction

Accurately simulating complex physical systems is vital for scientific discovery, but high-fidelity simulations are often prohibitively expensive to run at scale [7, 39, 50]. Surrogate models offer a practical alternative by learning from simulation outputs or observational data to deliver fast and accurate predictions [6, 9, 18, 25, 40, 42, 43]. This enables researchers to efficiently explore scientific phenomena, test hypotheses, and support decision-making. For example, climate scientists can use surrogate models to study how ocean temperatures respond to varying wind stress without repeatedly running costly simulations.

Implicit neural representations (INRs) provide a compact and continuous framework for surrogate modeling, particularly well-suited to spatially structured data. INRs typically use neural networks—most commonly multilayer perceptrons (MLPs) [6, 17, 28, 40, 44]—to learn a mapping from input coordinates (*e.g.*, spatial locations in the ocean) and simulation conditions (*e.g.*, wind stress amplitudes) directly to target variables (*e.g.*, temperature). This formulation enables resolution-independent, continuous predictions at arbitrary query points with a compact model size, making INRs an appealing choice for accelerating simulations.

Despite these advantages, applications of INRs in complex scientific domains often suffer from limited fidelity—particularly when modeling localized, high-frequency variations such as discontinuities or fine-scale structures that arise from underlying physical processes or complex boundary conditions [4, 14, 24, 33, 44]. To address this limitation, recent work augments INRs with learnable embeddings defined over rigid geometric structures (*e.g.*, grids) to explicitly encode complex spatial variations [5, 9, 15, 16, 45, 46]. In this setting, inputs to INRs are transformed into interpolated features

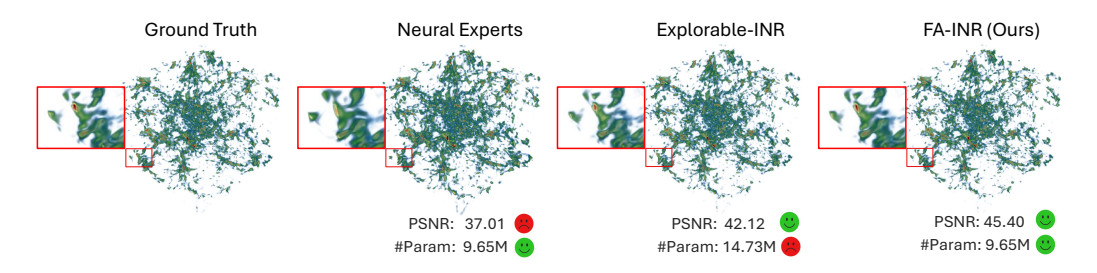


Figure 1: FA-INR outperforms alternative INR methods, including Neural Experts (a fully MLP-based INR) [3] and Explorable-INR (incorporating feature grids and planes) [9], while maintaining a compact model size.

retrieved from these embeddings. However, this approach compromises one of INRs' key strengths: *compact modeling*. Specifically, feature grids introduce significant memory overhead and scale poorly with increasing dimensionality and spatial resolution, even when low-rank approximations are used [5, 8, 15]. Moreover, data-independent rigid structures fail to adapt to data characteristics, often allocating excessive capacity to smooth regions while under-representing rapidly changing areas.

How can we preserve INRs' compactness while improving their fidelity in modeling scientific data?

Our proposal is to relax the rigid structural assumption. Specifically, unlike previous approaches, we bypass pre-defined positional structures (*e.g.*, grids) when augmenting INRs with learnable embeddings, enabling the model to allocate its capacity adaptively based on the data. We realize this idea using well-established cross-attention mechanisms [49] applied to a learnable, augmented key-value memory bank, inspired by the memory tokens in language modeling [21, 51, 52]. In this framework, grid-based embeddings emerge as a special case in which both the keys and interpolation weights are fixed a priori. By relaxing these constraints—and instead learning the keys alongside the values—our approach, **Feature-Adaptive INRs (FA-INR)**, unleashes the representational capacity of augmented embeddings. This flexibility enables the use of significantly more compact embeddings while achieving high-fidelity surrogate modeling, as illustrated in Figure 1.

To promote more effective use of the key-value pairs in the augmented memory bank—motivated by our observation that some pairs were rarely utilized—we propose specializing them for distinct spatial locations. We implement this idea using the Mixture of Experts (MoE) framework [10, 12, 13, 20, 36, 41], where the augmented key-value pairs are partitioned into multiple expert groups, and a routing mechanism is defined based on spatial coordinates. Given an input coordinate and simulation condition, our INR model first routes it to specific experts (*i.e.*, memory banks), then uses the retrieved value embedding as input to an MLP to predict the target variable. This design allows each expert to focus on dedicated subregions of the task space, enhancing feature extraction and improving embedding efficiency—particularly in modeling complex scientific data.

We validate our FA-INR on three large-scale ensemble simulation datasets across diverse domains: oceanography [22, 35], cosmology [1], and fluid dynamics [26]. Following the protocol in [9], we hold out a subset of simulation conditions as the test set and use the remainder for training and validation. Both quantitative and qualitative evaluations consistently show that our approach outperforms existing methods, achieving high-fidelity surrogate modeling with significantly smaller model sizes.

Our main contributions are three-fold:

- We propose FA-INR, an embedding-augmented INR that achieves high-fidelity surrogates with a compact model size. The novelty is in relaxing the rigid structural assumptions of prior work.
- We establish a novel connection between cross-attention over augmented memory and grid-based embedding augmentations, enabling a simple yet powerful implementation of FA-INR.
- We introduce a spatially-specialized memory mechanism based on MoE, allowing FA-INR to scale effectively to complex and large-scale simulation datasets. Additionally, we present a novel strategy for incorporating simulation conditions (*e.g.*, stress amplitudes), explicitly modeling the dependence of the target variable (*e.g.*, temperature) on the input simulation parameters.

## 2 Related Work

Surrogate Models for Scientific Simulations. Analyzing the real-world simulation systems across large parameter spaces often requires significant computational resources [7, 31]. To address this, numerous ML-based surrogate models [18, 39, 42, 50] have emerged in recent years. These approaches aim to accelerate scientific workflows and facilitate a deeper understanding of physical behaviors. For instance, the Fourier Neural Operator [23] was designed to approximate parametric PDEs efficiently for fluid dynamics problems. Similarly, MeshGraphNets [32], a graph neural network (GNN)-based method, was developed to deliver fast and accurate predictions for a variety of mesh-based physical simulations. Additionally, other works have focused on building surrogate models specifically for complex spatiotemporal simulation data [19, 25, 27]. Surrogate models, especially in the context of ensemble simulations where multiple outputs are generated under varying simulation parameters, require strong generalization ability. Recent climate-focused models, including ClimaX [30], a transformer-based model, and Spherical DYffusion [37], a generative model, were proposed to approximate the large-scale multivariate climate ensemble data. Moreover, GNN-Surrogate [43], developed for non-structured mesh data, employs a hierarchical architecture to efficiently predict high-dimensional outputs in ocean simulations.

Implicit Neural Representations. INRs have emerged as a powerful method for learning continuous and memory-efficient representations of scenes. Within this domain, multilayer perceptrons (MLPs) have frequently been utilized as the backbone architecture. These MLP-based models take input coordinates and map them to corresponding signal attributes [28, 38, 44, 47, 48]. However, MLP-based fully implicit models often struggle at accurately representing high-frequency details, such as edges and textures [33]. While various techniques such as positional encodings and specialized activation functions have been proposed to improve the performance of fully implicit models, another line of research has focused on integrating explicit data structures into the traditional frameworks [5, 15, 16, 29, 45, 46]. Those works using explicit representations further enhance the model efficiency and reconstruction quality.

**Mixture-of-Experts for INRs.** Recent research has increasingly adopted Mixture-of-Experts (MoE) to address the challenges of modeling large-scale scenes. However, many existing MoE frameworks designed for Neural Radiance Fields (NeRF) [11, 53] significantly differ from the objectives for traditional INR tasks [3, 34]. To bridge this gap and effectively adapt MoE principles to INRs, a recent work [3] learns local piecewise continuous functions for general implicit representations using MLP-based INR models. In contrast, our approach leverages the MoE idea only to the augmented memory banks and utilizes spatial locations as the routing signals.

## 3 INR-based Surrogate Models

#### 3.1 Preliminaries

**Problem definition.** We aim to develop a surrogate to model spatially structured scientific data generated by a numerical simulator. This kind of simulator typically produces data corresponding to a predefined set of spatial coordinates, denoted as  $X = \{x_1, x_2, ..., x_N\}$ , where each coordinate  $x_i \in \mathbb{R}^d$ . For given simulation parameters  $p_j \in \mathbb{R}^m$  (e.g., wind stress amplitudes), the simulator outputs a corresponding set of physical values  $Y_j = \{y_{j,1}, y_{j,2}, ..., y_{j,N}\}$  at X's locations.

Typically, simulation involves solving complex partial differential equations (PDEs) [31], easily requiring days to generate the data even for a small set of simulation parameters. The objective of a surrogate model is to learn an approximate mapping function  $g: \mathbb{R}^{N \times d} \times \mathbb{R}^m \to \mathbb{R}^N$ , such that given the coordinates X and the simulation parameters  $p_j$ , it can predict the corresponding output field  $Y_i$  significantly faster than the original simulators.

**INR for surrogate modeling.** An INR aims to learn this mapping using a neural network  $f_{\theta}$ , parameterized by weights  $\theta$ . Unlike traditional surrogate models that take the entire X as input to predict  $Y_j$  at once, an INR learns a function that maps a single input pair  $(x_i, p_j)$  to its target output  $y_{j,i}$ . That is,  $f_{\theta}: \mathbb{R}^d \times \mathbb{R}^m \to \mathbb{R}$ , such that  $f_{\theta}(x_i, p_j) \approx y_{j,i}$ . Without loss of generality, we assume  $y_{j,i}$  is a scalar value, but extending it to a vector is straightforward. Once the INR model is trained, it allows flexible querying at arbitrary coordinates and for arbitrary parameter sets.

Given a training dataset  $\mathcal{D} = \{(X, p_1, Y_1), (X, p_2, Y_2), ..., (X, p_J, Y_J)\}$  with J simulation runs, the INR model  $f_\theta$  can be trained by minimizing the following empirical risk:

$$\mathcal{L}(\theta) = \frac{1}{J \cdot N} \sum_{j=1}^{J} \sum_{i=1}^{N} \ell(f_{\theta}(x_i, p_j), y_{j,i}), \tag{1}$$

where  $\ell(\cdot)$  is the loss function, e.g., Mean Squared Error (MSE), which measures the differences between the predicted value  $f_{\theta}(x_i, p_j)$  and the truth value  $y_{j,i}$ .

## 3.2 Challenges

Limitations of INRs. While INR offers a compact approach for function approximation, it directly processes coordinates as inputs, making it struggle with modeling high-frequency variations [14, 33]. To address this, positional encoding techniques, such as Fourier mapping [28], are introduced to enable MLPs to better capture fine-grained details, where the input coordinate  $x_i$  is transformed to a higher-dimensional space via  $\gamma(x_i) = [\cos(2\pi\Omega x_i), \sin(2\pi\Omega x_i)]$ , with  $\Omega$  denoting the frequency matrix.

Explicit representations for INRs. Recent approaches further improve the representational power of INRs by incorporating explicit feature encodings [5, 15, 16, 45, 46] into the MLP-based framework, as illustrated in Figure 2. These encodings often employ structured representations, such as feature grids, which store learnable feature vectors at discrete locations (vertices). For example, for threedimensional input coordinates, a feature grid  $\mathcal{F} \in$  $\mathbb{R}^{N_1 \times N_2 \times N_3 \times D}$  can be utilized. Here,  $(N_1, N_2, N_3)$ defines the grid resolution, and D is the dimension of the feature vectors stored at each vertex. To obtain the feature vector  $z^{(x)}$  of an arbitrary input coordinate  $x \in \mathbb{R}^d$ , the coordinate x is first mapped from its original spatial domain to a normalized feature space  $[-1,1]^3$  through a linear projection  $\phi$ . Then,  $z^{(x)}$  is retrieved by interpolating the features stored at the neighboring vertices of x within the grid  $\mathcal{F}$ . The feature interpolation process can be defined as:

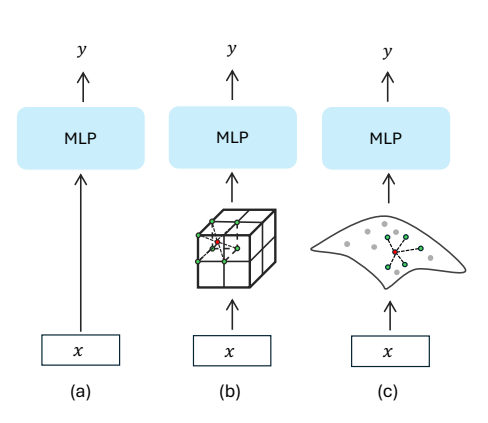


Figure 2: Architectures of three types of INR models: (a) Basic MLP-based INR, (b) INR with structured explicit representations, and (c) Our proposed Feature-Adaptive INR.

$$z^{(x)} = \psi(\mathcal{F}, \phi(x)). \tag{2}$$

While structured feature encodings, such as grids and planes, efficiently capture localized fine-grained details, achieving high-fidelity reconstructions typically requires dense representations, resulting in significant memory usage. This dense storage is often redundant, particularly for large-scale scientific datasets where smooth regions may present nearly uniform values. While in rapidly changing areas, these rigid data-independent structures may under-represent the underlying complexity.

# 4 Feature-Adaptive INR

To address the limitations of previous approaches, we proposed an adaptive INR with an augmented key-value memory bank, inspired by similar concepts in language modeling. The memory bank can be denoted by  $\{K \in \mathbb{R}^{M \times D_k}, V \in \mathbb{R}^{M \times D_v}\}$ , where K indicates a set of key vectors serve as feature locations, and V are the corresponding feature representations. By enabling both K and V to be learnable, thereby allowing the feature locations to be adaptive based on data characteristics rather than predefined locations, our approach makes more efficient and effective use of the augmented embeddings.

#### 4.1 Adaptive Encodings via Cross-Attention

To retrieve the feature representation from the augmented memory bank, we leverage the cross-attention mechanism. As illustrated in Figure 3-(a), each query vector  $q^{(x_i)}$  is produced from a spatial coordinate  $x_i$  via an encoder MLP  $f_{\theta_E}$ , parameterized by  $\theta_E$ . Specifically,  $f_{\theta_E}$  first maps  $x_i$  to an

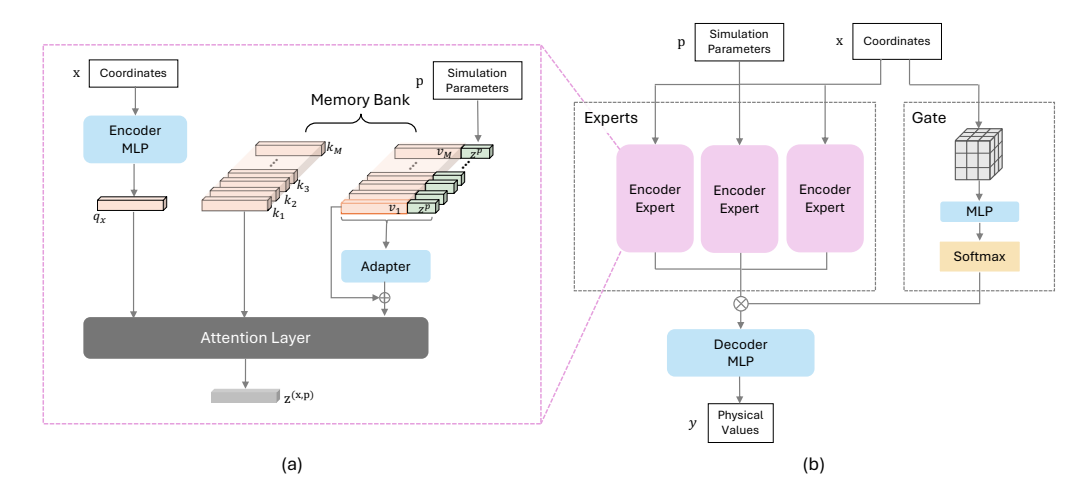


Figure 3: Architecture of the proposed FA-INR. An input pair (x, p) is first routed by a gating mechanism in (b) to the most relevant spatially-specialized expert encoders (see (a)). Then, the aggregated feature vector from all selected experts is further processed by the MLP decoder in (b).

intermediate feature vector  $z^{(x_i)}$ . This vector is then projected into a query representation via a linear mapping. Formally, this encoding process is defined as:

$$z^{(x_i)} = f_{\theta_E}(x_i),$$

$$q^{(x_i)} = z^{(x_i)} W_q, \ W_q \in \mathbb{R}^{D_q \times D_k},$$
(3)

where  $\theta_E$  is the weights of the encoder MLP and  $W_q$  is a learnable projection matrix mapping the intermediate spatial features to the query dimension  $D_k$ .

Each spatial query dynamically retrieves the corresponding feature from the memory bank via cross-attention, similar to the interpolation process defined in Equation 2, but in a learnable and data-adaptive manner. The attention-based feature interpolation is computed as:

$$z^{(x_i, p_j)} = \operatorname{Softmax}\left(\frac{q^{(x_i)}(KW_k)^{\top}}{\sqrt{D_k}}\right) V^{(X, P)} W_v, \tag{4}$$

where  $W_k \in \mathbb{R}^{D_k \times D_k}$  and  $W_v \in \mathbb{R}^{D_v \times D_v}$  are learnable linear projection matrices applied to keys and values, respectively. Here,  $V^{(X,P)}$  represents parameter-conditioned embeddings obtained through a value adapter  $f_{\theta_A}$ .

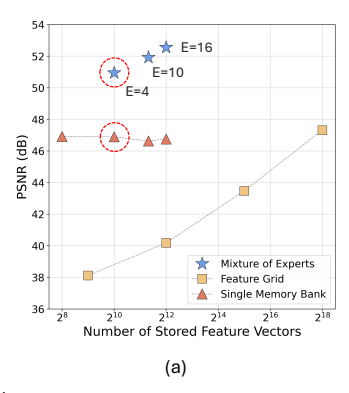
Specifically, to effectively incorporate the simulation parameters into the feature retrieval process, each simulation condition is represented by a vector  $p_j$ , where each element  $s \in S$  denotes an individual scalar parameter within  $p_j$ . Each scalar  $s \in S$  is first individually embedded into a one-dimensional feature vector  $z_s^{(p_j)}$ . These scalar-level embeddings are then combined via an element-wise (Hadamard) product [9, 15] to form a unified parameter embedding  $z^{(p_j)}$ , which better preserves the signal from each individual parameter. As shown in Figure 3, this integrated embedding is then concatenated with each retrieved value in the memory bank and further processed by the adapter  $f_{\theta_A}$ :

$$V^{(X,P)} = V + f_{\theta_{A}}(V \oplus z^{(p_{j})}),$$
where  $z^{(p_{j})} = \odot_{s \in S} z_{s}^{(p_{j})}.$  (5)

This residual connection is designed to better preserve the original spatial information while explicitly adapting the features based on the specific simulation parameters  $p_j$ .

## 4.2 Scaling up FA-INR

As illustrated in Figure 4-(a), using a single small memory bank, our approach can already outperform the grid-based approach. Intuitively, we would expect that enlarging the memory bank by adding more key-value pairs would achieve further improvements. However, as shown in Figure 4-(a), merely increasing the size of the memory bank results in limited performance gains or even slight



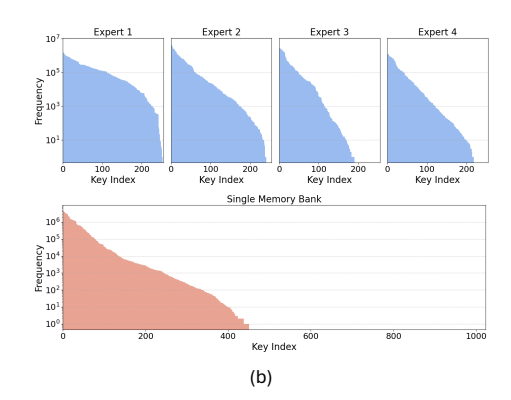


Figure 4: Comparison of scalability among three strategies on the MPAS-Ocean dataset. (a) Our FA-INR using MoE can effectively scale up the performance than solely expanding the memory bank size, while requiring fewer feature vectors compared to the grid-based method. The comparison of two histograms in (b) demonstrates that using MoE leads to more effective key utilization.

degradation. With a closer inspection, we found out that many key-value pairs are rarely utilized. Specifically, we trace the top-8 keys activated by each coordinate  $x_i$  and summarize their usage in histograms. As shown in the bottom part of Figure 4-(b), a significant portion of keys are rarely used.

We hypothesize that this inefficient usage is caused by the random initialization of keys and values, which makes some pairs out of range to be retrieved. To address this issue, we propose to impose additional constraints to specialize key-value pairs into groups, and use the spatial location  $x_i$  as the routing signal to determine which group of memory banks to query. This strategy just aligns with the idea of Mixture-of-Experts (MoE).

As illustrated in Figure 3-(b), each expert in our framework is an attention-based feature encoder associated with a memory bank. To dynamically select the most relevant experts for each coordinate  $x_i$ , we introduce a gating mechanism, consisting of two key components: a small, low-resolution feature grid  $\mathcal{F}_G$  to provide a coarse spatial representation, and a small MLP  $f_{\theta_G}$  parameterized by  $\theta_G$ . Given an input coordinate  $x_i$ , its corresponding coarse spatial feature  $z_G^{(x_i)}$  is first extracted from  $\mathcal{F}_G$ . This feature vector is then processed by the small MLP  $f_{\theta_G}$ . Finally, a softmax function is applied to the output to produce the expert selection probabilities:

$$\Phi(x_i) = \operatorname{softmax}(f_{\theta_G}(z_G^{(x_i)})), \ \Phi(x_i) \in \mathbb{R}^E.$$
(6)

Here, E represents the total number of expert modules, and  $\Phi(x_i)$  is the probability distribution over these encoding experts.

#### 4.3 Overall Framework of FA-INR

**Mixture of encoder experts.** Given the gating probabilities  $\Phi(x_i)$ , the top-K expert encoders will be selected for each coordinate  $x_i$ . The final aggregated feature  $\bar{z}^{(x_i,p_j)}$  is then computed as a weighted sum of the feature vectors  $z_k^{(x_i,p_j)}$  produced by the selected experts:

$$\bar{z}^{(x_i, p_j)} = \sum_{k=1}^{K} \Phi(x_i)_k \cdot z_k^{(x_i, p_j)}, \tag{7}$$

where  $\Phi(x_i)_k$  is the probability of routing  $x_i$  to the k-th expert, and  $z_k^{(x_i,p_j)}$  represents the corresponding output feature vector from the k-th expert encoder, conditioned on both the spatial coordinate  $x_i$  and the simulation parameter  $p_j$ .

**Feature decoder.** To decode the feature vector  $\bar{z}^{(x_i,p_j)}$  into a physical scalar value, we employ a small MLP as a feature decoder,  $f_{\theta_D}$ , parameterized by  $\theta_D$ . This decoder maps the feature vector to the predicted physical value  $\hat{y}_{j,i}$ :

$$\hat{y}_{j,i} = f_{\theta_{\mathcal{D}}}(\bar{z}^{(x_i, p_j)}). \tag{8}$$

**Optimization.** The entire FA-INR, including all encoder experts, the gating network, and the final feature decoder, is trained in an end-to-end manner. The optimization objective is to minimize

the Mean Squared Error (MSE) loss between the predicted scalar values  $\hat{y}_{j,i}$  and the ground-truth values  $y_{j,i}$ , computed across all J ensemble members and N coordinates. The training objective is formulated as follows:

$$\mathcal{L}_{MSE}(\theta) = \frac{1}{J \cdot N} \sum_{i=1}^{J} \sum_{i=1}^{N} \left\| f_{\theta_{D}}(\bar{z}^{(x_{i}, p_{j})}) - y_{j, i} \right\|_{2}^{2}, \tag{9}$$

where  $\theta$  represents all learnable parameters of the model, and  $y_{j,i}$  is the ground-truth scalar value at coordinate  $x_i$  for the j-th simulation run in the ensemble dataset.

# 5 Experiments

#### 5.1 Experimental Settings

**Datasets.** We conduct the experiments on three real-world ensemble simulation datasets. (1) *MPASOcean* [35]: A global ocean system simulation data defined in spherical coordinates (*i.e.*, latitude, longitude, and depth), capturing corresponding ocean temperature values. (2) *Nyx* [1]: A cosmological hydrodynamics simulation dataset with structured spatial locations and associated dark matter density measurements. (3) *CloverLead3D* [26]: A fluid dynamics simulation dataset with structured locations and corresponding energy values. Additional dataset information, including the number of ensemble members for training and testing, the number of spatial coordinates, and the number of simulation variables, is shown in Table 1. Further details about each dataset will be provided in Appendix A.

Table 1: Scientific ensemble simulation datasets and training setups.

Dataset	Simulation Parameters	Spatial Coordinates	Training Fields	Test Fields
MPAS-Ocean	4	11,845,146	70	30
Nyx	3	$512^{3}$	100	30
CloverLeaf	6	$128^{3}$	500	100

**Baselines.** We compare FA-INR with four baseline INR approaches. (1) K-Planes [15] represents arbitrary-dimensional data by factorizing it into multiple 2D feature planes, providing a flexible and efficient modeling approach. (2) MMGN [25] proposes a novel context-aware indexing mechanism and a set of multiplicative basis functions for high-quality physical fields reconstruction from sparse observations. (3) Neural Experts [3] enhances the capability of MLP-based SIREN [44] by leveraging the MoE architecture to learn local piece-wise continuous approximations. (4) Explorable-INR [9] combines one feature grid and multiple 2D planes to balance the model efficiency and accuracy, which is a strong baseline method specifically designed for ensemble simulations.

**Evaluation metrics.** We evaluate the performance of surrogate models using three metrics. Peak Signal-to-Noise Ratio (PSNR) quantifies the numerical difference between predicted scalar values and ground-truth simulation outputs, where higher PSNR indicates more accurate approximations of the true signals. Additionally, normalized maximum difference (MD) [9, 43] is utilized to estimate the error bounds. To measure the visual fidelity, we render both predicted and ground-truth 3D fields into 2D images using the same viewpoints and rendering settings, and then compute the Structural Similarity Index Measure (SSIM) to quantify their perceptual similarity.

Implementation and training details. We employ the same architectural configuration for the MPAS-Ocean and CloverLeaf datasets, while slightly increasing the model complexity for the Nyx dataset. Specifically, we use 256 key-value pairs in the memory bank for MPAS-Ocean and CloverLeaf, and 1,024 pairs for Nyx. To ensure fair comparisons, we also scale up the models of Neural Experts and MMGN by increasing their network depth and hidden dimensions to match the sizes of our models. This adjustment is necessary since both methods were originally designed for relatively simpler scenarios, such as 2D data or non-scientific scenes. Additionally, we keep the original configuration of Explorable-INR and control the dimensions of our spatial and simulation parameter embeddings to match those used in their model. For our MoE implementation, we choose Top-2 routing to balance computational efficiency and accuracy. Additional implementation details of FA-INR are provided in Appendix C.

Table 2: Quantitative comparison of the proposed FA-INR with four baseline INR methods across the MPAS-Ocean, Nyx, and CloverLeaf3D datasets.

Dataset	Model	#Experts	#Params	PSNR↑	SSIM↑	MD↓
•	FA-INR (Ours)	10	1.10M	51.92	0.9934	0.1536
	Explorable-INR	-	7.38M	49.45	0.9908	0.1917
MPAS-Ocean	K-Planes	-	43.17M	44.01	0.9897	0.1643
	Neural Experts	10	1.10M	41.10	0.9822	0.3403
	MMGN	-	1.10M	43.03	0.9856	0.2406
	FA-INR (Ours)	8	9.65M	44.72	0.9575	0.0835
	Explorable-INR	-	14.73M	42.59	0.9415	0.1162
Nyx	K-Planes	-	40.63M	34.99	0.8923	0.1663
	Neural Experts	8	9.65M	37.84	0.9212	0.1720
	MMGN	-	9.65M	39.81	0.9288	0.2078
	FA-INR (Ours)	10	1.10M	53.79	0.9694	0.0482
CloverLeaf	Explorable-INR	-	7.38M	48.92	0.9465	0.0560
	K-Planes	-	6.79M	46.82	0.9393	0.0611
	Neural Experts	10	1.10M	53.38	0.9678	0.0618
	MMGN	-	1.10M	45.51	0.9311	0.0698

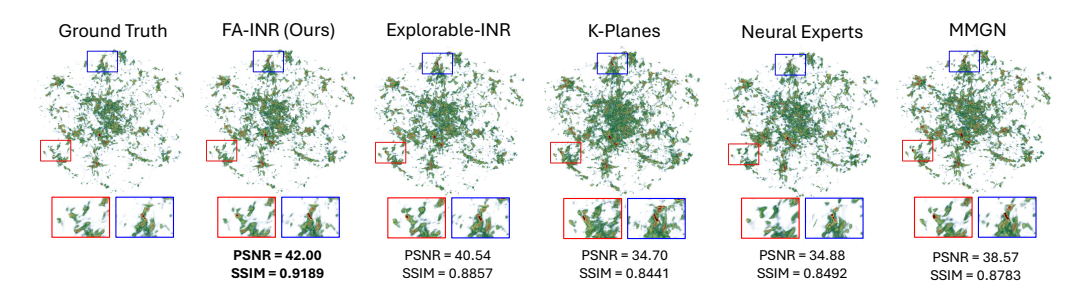


Figure 5: Rendering results comparing the qualitative performance of our proposed FA-INR with four baseline INR models. The selected test instance from the Nyx dataset presents significant challenges in modeling its complex cosmological features.

### 5.2 Main Results

We follow the experimental protocols from prior surrogate modeling work [9, 43] to mainly study how the model performs given sets of new simulation parameters. We also conduct experiments to evaluate how FA-INR can generalize to a set of unseen locations (*e.g.*, new sensor locations), and those results can be found in Appendix G.

**Improved model quality.** The quantitative evaluation across all three datasets is summarized in Table 2. Overall, our proposed FA-INR consistently achieves the highest performance compared to all baseline approaches. Specifically, FA-INR outperforms the other baselines by 17.49% in PSNR on the MPAS-Ocean dataset, 15.83% on the Nyx dataset, and 10.95% on the CloverLeaf3D dataset. Moreover, FA-INR achieves the lowest maximum difference (MD) values across all three datasets, which indicates that our model is more effective at minimizing the large, critical prediction errors, making it more reliable for scientists to conduct parameter-space explorations.

Reduced model sizes. While Explorable-INR achieves competitive performance, it employs one feature grid  $(64^3)$  and three high-resolution 2D planes  $(3 \times 256^2)$ , resulting in a significantly larger model size compared to our method, particularly for the MPAS-Ocean and CloverLeaf datasets. In contrast, our proposed FA-INR not only utilizes fewer network parameters but also achieves higher prediction quality. Furthermore, since K-Planes decomposes the input space into combinations of all possible pairs of variables and approximates each using a multi-resolution design, it inevitably requires significantly more network parameters compared to all the other methods. This issue is particularly pronounced for modeling ensemble simulation data, where the simulation parameters introduce additional dimensions beyond those typically encountered in general 3D scenarios.

**Improved visual fidelity.** To showcase the high visual fidelity of our proposed FA-INR, we present qualitative comparisons on a test field from the Nyx dataset in Figure 5. Overall, K-Planes exhibits notably poor performance in both numerical metrics and visual quality. As shown in the zoomed-in images, we found that K-Planes introduces numerous artifacts. These issues could be attributed to

two reasons. First, the cosmology data contains highly complex features in the 3D space, which can be challenging to approximate solely using 2D representations. Second, the use of multi-resolution data structures could further amplify those false features. Furthermore, Neural Experts fails to capture high-frequency details, as shown in the left zoomed-in image. This limitation likely comes from its underlying MLP-based architecture, which lacks sufficient capacity to accurately represent complex features existing in the high-dimensional scientific data. Additional visual analyses for MPAS-Ocean and CloverLeaf datasets are provided in Appendix D.

#### 5.3 Ablation Study

**Design choices for spatial encoding.** To verify the impact of architectures used for spatial encoding, we conduct ablation studies on the Nyx dataset. We replaced the memory bank (*i.e.*, 1,024 key-value pairs per bank) with alternative structures: a feature grid, three feature planes, or an MLP with the Sine activation. To ensure fair comparisons, we maintained *a consistent number of model parameters across all designs*. For the three alternative structures, simulation parameter information is integrated using a separate embedding, which is then concatenated with the spatial embedding to serve as inputs to the decoder. Moreover, we also conduct experiments to replace our proposed value adapter with the embedding concatenation. All the results are presented in Table 3. Specifically, with a controlled model size, both feature grid and plane achieve even worse performance compared to MLP, indicating that their effectiveness heavily relies on dense representations. It is important to note that the MLP-based design can achieve acceptable performance here mainly because the MLP was dedicated solely to spatial encoding, while traditional methods take a concatenation of raw spatial coordinates and simulation parameters directly into the MLP.

Table 3: Ablation study on alternative architectures for spatial encoding. Experiments are conducted on the Nyx dataset, both with and without the integration of a Mixture of Experts (MoE) framework.

Design	Memo w/ Adapter	Grid	Plane	MLP	
w/o MoE PSNR↑ MD↓	39.49 0.0976	38.98 0.1281	36.69 0.1656	33.41 0.1896	38.19 0.1258
#Experts PSNR↑ MD↓	8 44.72 0.0835	8 44.05 0.1028	8 41.10 0.1389	8 38.77 0.1408	8 42.77 0.1204

Number of experts. We investigate the impact of increasing the number of encoding experts on model performance. In the experiments, all experts share the same architecture, and each coordinate is routed to the top-2 experts. As shown in Table 4, increasing the number of experts significantly improves performance on the MPAS-Ocean dataset. However, the performance gain becomes relatively small beyond using 10 experts, with a degradation in the MD score. A similar trend is observed for the Nyx dataset: increasing the expert number from 10 to 12 only provides a marginal improvement in PSNR, but with a decrease in the MD metric. It is important to note that the MoE framework in FA-INR is applied solely to the feature encoding component rather than the entire INR architecture. Therefore, increasing the number of experts will not substantially increase the training time and model size. Additional analysis for the MoE components, including the gating network and expert assignment, is included in Appendix E.

Table 4: Ablation study on the number of encoding experts.

Dataset	MPAS-Ocean			Nyx				
# Experts	1	4	10	16	1	8	10	12
# Params PSNR↑ MD↓	0.20M 46.92 0.2096	0.50M 50.94 0.1674	1.10M 51.92 <b>0.1536</b>	1.69M <b>52.55</b> 0.1774	1.36M 39.49 0.0976	9.65M 44.72 0.0835	12.02M 45.63 <b>0.0715</b>	14.39M <b>45.67</b> 0.0767

## 6 Conclusion

We introduce Feature-Adaptive INR (FA-INR), a compact, embedding-augmented implicit neural representation designed for high-fidelity surrogate modeling of scientific ensemble simulations. To

overcome the rigidity of prior explicit data structures, we propose an adaptive encoding approach leveraging cross-attention with an augmented memory bank. For scalability to complex, large-scale scientific datasets, we integrate a Mixture-of-Experts (MoE) framework that dynamically routes inputs to relevant memory banks based on their spatial data characteristics. Comprehensive evaluations have demonstrated that FA-INR achieves state-of-the-art fidelity surrogate modeling.

# References

- [1] Ann S Almgren, John B Bell, Mike J Lijewski, Zarija Lukić, and Ethan Van Andel. Nyx: A massively parallel amr code for computational cosmology. *The Astrophysical Journal*, 765(1):39, 2013.
- [2] Utkarsh Ayachit. The paraview guide: a parallel visualization application. Kitware, Inc., 2015.
- [3] Yizhak Ben-Shabat, Chamin Hewa Koneputugodage, Sameera Ramasinghe, and Stephen Gould. Neural experts: Mixture of experts for implicit neural representations. *Advances in Neural Information Processing Systems*, 37:101641–101670, 2024.
- [4] Johannes Brandstetter, Daniel Worrall, and Max Welling. Message passing neural pde solvers. *arXiv* preprint arXiv:2202.03376, 2022.
- [5] Ang Cao and Justin Johnson. Hexplane: A fast representation for dynamic scenes. In Proceedings of the IEEE/CVF Conference on Computer Vision and Pattern Recognition, pages 130–141, 2023.
- [6] Giovanni Catalani, Siddhant Agarwal, Xavier Bertrand, Frédéric Tost, Michael Bauerheim, and Joseph Morlier. Neural fields for rapid aircraft aerodynamics simulations. *Scientific Reports*, 14(1):25496, 2024.
- [7] Nicolas Chartier, Benjamin Wandelt, Yashar Akrami, and Francisco Villaescusa-Navarro. Carpool: fast, accurate computation of large-scale structure statistics by pairing costly and cheap cosmological simulations. Monthly Notices of the Royal Astronomical Society, 503(2):1897–1914, 2021.
- [8] Anpei Chen, Zexiang Xu, Andreas Geiger, Jingyi Yu, and Hao Su. Tensorial radiance fields. In *European conference on computer vision*, pages 333–350. Springer, 2022.
- [9] Yi-Tang Chen, Neng Shi, Xihaier Luo, Wei Xu, and Han-Wei Shen. Explorable inr: an implicit neural representation for ensemble simulation enabling efficient spatial and parameter exploration. *IEEE Transactions on Visualization and Computer Graphics*, 2025.
- [10] Zixiang Chen, Yihe Deng, Yue Wu, Quanquan Gu, and Yuanzhi Li. Towards understanding the mixture-of-experts layer in deep learning. Advances in neural information processing systems, 35:23049–23062, 2022.
- [11] Francesco Di Sario, Riccardo Renzulli, Enzo Tartaglione, and Marco Grangetto. Boost your nerf: A model-agnostic mixture of experts framework for high quality and efficient rendering. In *European Conference on Computer Vision*, pages 176–192. Springer, 2024.
- [12] Nan Du, Yanping Huang, Andrew M Dai, Simon Tong, Dmitry Lepikhin, Yuanzhong Xu, Maxim Krikun, Yanqi Zhou, Adams Wei Yu, Orhan Firat, et al. Glam: Efficient scaling of language models with mixture-of-experts. In *International conference on machine learning*, pages 5547–5569. PMLR, 2022.
- [13] William Fedus, Jeff Dean, and Barret Zoph. A review of sparse expert models in deep learning. *arXiv* preprint arXiv:2209.01667, 2022.
- [14] Sara Fridovich-Keil, Raphael Gontijo Lopes, and Rebecca Roelofs. Spectral bias in practice: The role of function frequency in generalization. Advances in Neural Information Processing Systems, 35:7368–7382, 2022.
- [15] Sara Fridovich-Keil, Giacomo Meanti, Frederik Rahbæk Warburg, Benjamin Recht, and Angjoo Kanazawa. K-planes: Explicit radiance fields in space, time, and appearance. In *Proceedings of the IEEE/CVF Conference on Computer Vision and Pattern Recognition*, pages 12479–12488, 2023.
- [16] Sara Fridovich-Keil, Alex Yu, Matthew Tancik, Qinhong Chen, Benjamin Recht, and Angjoo Kanazawa. Plenoxels: Radiance fields without neural networks. In *Proceedings of the IEEE/CVF conference on computer vision and pattern recognition*, pages 5501–5510, 2022.
- [17] Jun Han and Chaoli Wang. Coordnet: Data generation and visualization generation for time-varying volumes via a coordinate-based neural network. *IEEE Transactions on Visualization and Computer Graphics*, 29(12):4951–4963, 2022.
- [18] Wenbin He, Junpeng Wang, Hanqi Guo, Ko-Chih Wang, Han-Wei Shen, Mukund Raj, Youssef SG Nashed, and Tom Peterka. Insitunet: Deep image synthesis for parameter space exploration of ensemble simulations. *IEEE transactions on visualization and computer graphics*, 26(1):23–33, 2019.
- [19] Chuanbo Hua, Federico Berto, Michael Poli, Stefano Massaroli, and Jinkyoo Park. Learning efficient surrogate dynamic models with graph spline networks. *Advances in Neural Information Processing Systems*, 36:52523–52547, 2023.

- [20] Robert A Jacobs, Michael I Jordan, Steven J Nowlan, and Geoffrey E Hinton. Adaptive mixtures of local experts. *Neural computation*, 3(1):79–87, 1991.
- [21] Guillaume Lample, Alexandre Sablayrolles, Marc'Aurelio Ranzato, Ludovic Denoyer, and Hervé Jégou. Large memory layers with product keys. Advances in Neural Information Processing Systems, 32, 2019.
- [22] Adam Larios, Mark R Petersen, and Collin Victor. Application of continuous data assimilation in high-resolution ocean modeling. arXiv preprint arXiv:2308.02705, 2023.
- [23] Zongyi Li, Nikola Kovachki, Kamyar Azizzadenesheli, Burigede Liu, Kaushik Bhattacharya, Andrew Stuart, and Anima Anandkumar. Fourier neural operator for parametric partial differential equations. arXiv preprint arXiv:2010.08895, 2020.
- [24] Lu Lu, Pengzhan Jin, Guofei Pang, Zhongqiang Zhang, and George Em Karniadakis. Learning nonlinear operators via deeponet based on the universal approximation theorem of operators. *Nature machine* intelligence, 3(3):218–229, 2021.
- [25] Xihaier Luo, Wei Xu, Balu Nadiga, Yihui Ren, and Shinjae Yoo. Continuous field reconstruction from sparse observations with implicit neural networks. In *The Twelfth International Conference on Learning Representations*, 2024.
- [26] Andrew Mallinson, David A Beckingsale, Wayne Gaudin, J Herdman, John Levesque, and Stephen A Jarvis. Cloverleaf: Preparing hydrodynamics codes for exascale. *The Cray User Group*, 2013, 2013.
- [27] Michael McCabe, Bruno Régaldo-Saint Blancard, Liam Parker, Ruben Ohana, Miles Cranmer, Alberto Bietti, Michael Eickenberg, Siavash Golkar, Geraud Krawezik, Francois Lanusse, et al. Multiple physics pretraining for spatiotemporal surrogate models. Advances in Neural Information Processing Systems, 37:119301–119335, 2024.
- [28] Ben Mildenhall, Pratul P Srinivasan, Matthew Tancik, Jonathan T Barron, Ravi Ramamoorthi, and Ren Ng. Nerf: Representing scenes as neural radiance fields for view synthesis. *Communications of the ACM*, 65(1):99–106, 2021.
- [29] Thomas Müller, Alex Evans, Christoph Schied, and Alexander Keller. Instant neural graphics primitives with a multiresolution hash encoding. *ACM transactions on graphics (TOG)*, 41(4):1–15, 2022.
- [30] Tung Nguyen, Johannes Brandstetter, Ashish Kapoor, Jayesh K Gupta, and Aditya Grover. Climax: A foundation model for weather and climate. arXiv preprint arXiv:2301.10343, 2023.
- [31] Ruben Ohana, Michael McCabe, Lucas Meyer, Rudy Morel, Fruzsina Agocs, Miguel Beneitez, Marsha Berger, Blakesly Burkhart, Stuart Dalziel, Drummond Fielding, et al. The well: a large-scale collection of diverse physics simulations for machine learning. Advances in Neural Information Processing Systems, 37:44989–45037, 2024.
- [32] Tobias Pfaff, Meire Fortunato, Alvaro Sanchez-Gonzalez, and Peter Battaglia. Learning mesh-based simulation with graph networks. In *International conference on learning representations*, 2020.
- [33] Nasim Rahaman, Aristide Baratin, Devansh Arpit, Felix Draxler, Min Lin, Fred Hamprecht, Yoshua Bengio, and Aaron Courville. On the spectral bias of neural networks. In *International conference on machine learning*, pages 5301–5310. PMLR, 2019.
- [34] Daniel Rebain, Wei Jiang, Soroosh Yazdani, Ke Li, Kwang Moo Yi, and Andrea Tagliasacchi. Derf: Decomposed radiance fields. In *Proceedings of the IEEE/CVF Conference on Computer Vision and Pattern Recognition*, pages 14153–14161, 2021.
- [35] Todd Ringler, Mark Petersen, Robert L Higdon, Doug Jacobsen, Philip W Jones, and Mathew Maltrud. A multi-resolution approach to global ocean modeling. *Ocean Modelling*, 69:211–232, 2013.
- [36] Carlos Riquelme, Joan Puigcerver, Basil Mustafa, Maxim Neumann, Rodolphe Jenatton, André Susano Pinto, Daniel Keysers, and Neil Houlsby. Scaling vision with sparse mixture of experts. Advances in Neural Information Processing Systems, 34:8583–8595, 2021.
- [37] Salva Rühling Cachay, Brian Henn, Oliver Watt-Meyer, Christopher S Bretherton, and Rose Yu. Probablistic emulation of a global climate model with spherical dyffusion. *Advances in Neural Information Processing* Systems, 37:127610–127644, 2024.
- [38] Vishwanath Saragadam, Daniel LeJeune, Jasper Tan, Guha Balakrishnan, Ashok Veeraraghavan, and Richard G Baraniuk. Wire: Wavelet implicit neural representations. In *Proceedings of the IEEE/CVF Conference on Computer Vision and Pattern Recognition*, pages 18507–18516, 2023.
- [39] Tapio Schneider, L Ruby Leung, and Robert CJ Wills. Opinion: Optimizing climate models with process knowledge, resolution, and artificial intelligence. Atmospheric Chemistry and Physics, 24(12):7041–7062, 2024
- [40] Louis Serrano, Lise Le Boudec, Armand Kassaï Koupaï, Thomas X Wang, Yuan Yin, Jean-Noël Vittaut, and Patrick Gallinari. Operator learning with neural fields: Tackling pdes on general geometries. Advances in Neural Information Processing Systems, 36:70581–70611, 2023.

- [41] Noam Shazeer, Azalia Mirhoseini, Krzysztof Maziarz, Andy Davis, Quoc Le, Geoffrey Hinton, and Jeff Dean. Outrageously large neural networks: The sparsely-gated mixture-of-experts layer. arXiv preprint arXiv:1701.06538, 2017.
- [42] Neng Shi, Jiayi Xu, Haoyu Li, Hanqi Guo, Jonathan Woodring, and Han-Wei Shen. Vdl-surrogate: A view-dependent latent-based model for parameter space exploration of ensemble simulations. *IEEE Transactions on Visualization and Computer Graphics*, 29(1):820–830, 2022.
- [43] Neng Shi, Jiayi Xu, Skylar W Wurster, Hanqi Guo, Jonathan Woodring, Luke P Van Roekel, and Han-Wei Shen. Gnn-surrogate: A hierarchical and adaptive graph neural network for parameter space exploration of unstructured-mesh ocean simulations. *IEEE Transactions on Visualization and Computer Graphics*, 28(6):2301–2313, 2022.
- [44] Vincent Sitzmann, Julien Martel, Alexander Bergman, David Lindell, and Gordon Wetzstein. Implicit neural representations with periodic activation functions. Advances in neural information processing systems, 33:7462–7473, 2020.
- [45] Cheng Sun, Min Sun, and Hwann-Tzong Chen. Direct voxel grid optimization: Super-fast convergence for radiance fields reconstruction. In *Proceedings of the IEEE/CVF conference on computer vision and* pattern recognition, pages 5459–5469, 2022.
- [46] Cheng Sun, Min Sun, and Hwann-Tzong Chen. Improved direct voxel grid optimization for radiance fields reconstruction. arXiv preprint arXiv:2206.05085, 2022.
- [47] Matthew Tancik, Ben Mildenhall, Terrance Wang, Divi Schmidt, Pratul P Srinivasan, Jonathan T Barron, and Ren Ng. Learned initializations for optimizing coordinate-based neural representations. In *Proceedings of the IEEE/CVF conference on computer vision and pattern recognition*, pages 2846–2855, 2021.
- [48] Matthew Tancik, Pratul Srinivasan, Ben Mildenhall, Sara Fridovich-Keil, Nithin Raghavan, Utkarsh Singhal, Ravi Ramamoorthi, Jonathan Barron, and Ren Ng. Fourier features let networks learn high frequency functions in low dimensional domains. *Advances in neural information processing systems*, 33:7537–7547, 2020.
- [49] Ashish Vaswani, Noam Shazeer, Niki Parmar, Jakob Uszkoreit, Llion Jones, Aidan N Gomez, Łukasz Kaiser, and Illia Polosukhin. Attention is all you need. Advances in neural information processing systems, 30, 2017.
- [50] Chenlu Wang, Junfeng Li, Zeping Wu, Jianhong Sun, Shuaichao Ma, and Yi Zhao. A surrogate modeling method for large-scale flow field prediction based on locally optimal shape parameters. Aerospace Traffic and Safety, 2025.
- [51] Yuhuai Wu, Markus N Rabe, DeLesley Hutchins, and Christian Szegedy. Memorizing transformers. arXiv preprint arXiv:2203.08913, 2022.
- [52] Yizhe Zhang and Deng Cai. Linearizing transformer with key-value memory. *arXiv preprint* arXiv:2203.12644, 2022.
- [53] MI Zhenxing and Dan Xu. Switch-nerf: Learning scene decomposition with mixture of experts for large-scale neural radiance fields. In *The Eleventh International Conference on Learning Representations*, 2022.

# **A** Experimental Datasets

In this section, we provide more details on the settings of simulation conditions.

**MPAS-Ocean** [35] is a simulation dataset of the global ocean system. It is characterized by four key input parameters: Bulk Wind Stress Amplification (*BwsA*), Critical Bulk Richardson Number (*CbrN*), Gent-McWilliams eddy transport coefficient (*GM*), and Horizontal Viscosity (*HV*). This dataset comprises 100 simulation instances, each corresponding to a unique combination of these four simulation parameters. These are divided into 70 instances for training and 30 for testing.

Nyx [1] is developed from the cosmological hydrodynamics simulations. This cosmology ensemble dataset was generated by using the following three simulation parameters: the total density of baryons (OmB), the total matter density (OmM), and the Hubble Constant (h). We use 100 instances for training and 30 instances for testing.

**CloverLeaf3D** [26] is a hydrodynamics simulation dataset generated by solving the 3D compressible Euler equations. This dataset focuses on six simulation parameters: three density parameters and three energy parameters. In the experiments, we randomly sample 500 instances for training and 100 instances for testing.

# **B** Terminology

In this section, we want to provide further explanations on the terms used in our paper. We define a "field" as the collection of physical values at predefined spatial locations, generated by a simulation run with a specific set of input simulation parameters. Within the scientific ensemble dataset, "ensemble instance" or "ensemble member" refers to a single such field.

In Table 1, terms like "training fields" or "test fields" represent the total number of ensemble instances sampled for training or testing. For example, "30 test fields from the Nyx dataset" denotes that 30 distinct fields were used for testing. Each of these test fields was generated using a unique set of simulation parameters. For the Nyx dataset, each simulation parameter set includes three variables, as detailed under the "simulation parameters" heading in Table 1.

## C Experimental Details

#### C.1 Implementations and Training Details

All models and experiments are implemented in PyTorch and conducted on NVIDIA A100 GPUs. For the MPAS-Ocean and CloverLeaf datasets, we use a one-hidden-layer encoder MLP with Sine activation (as shown in Figure 3-a), while for the Nyx dataset, a deeper encoder MLP with four hidden layers is employed. For all three datasets, the value adapter in the memory bank is implemented using a two-layer MLP. Additionally, all datasets share the same decoder MLP architecture (shown in Figure 3-b), consisting of three layers with ReLU activation. Other implementation details are introduced in subsection 5.1.

All models were optimized using the Adam optimizer and the mean squared error (MSE) as the training objective. During training, we randomly selected 25% of the input pairs consisting of spatial coordinates and simulation parameters (as defined in subsection 3.1) to be the validation set. The initial learning rate was set to  $1\times10^{-4}$  with a decay rate of 10%. For Neural Experts, which utilize a fully MLP-based architecture, we employed a lower learning rate of  $1\times10^{-6}$  to ensure training stability on the Nyx dataset. Moreover, all models are optimized using a consistent batch size for fair comparisons.

#### **C.2** Details on Embedding the Simulation Parameters

As introduced in subsection 4.1, we propose a value adapter designed to integrate simulation parameters directly into the feature retrieval process. This approach ensures that the feature vectors output by the attention module are already parameter-conditioned, allowing them to be directly forwarded to the feature decoder.

In an ablation study (detailed in Table 3), we investigate whether using the value adapter enhances model performance compared to an alternative method: treating the simulation parameter features  $(z^{(p_j)})$  as an independent embedding. This alternative strategy is also employed for the grid, plane, and MLP-based implementations (as shown in Table 3), where the independent parameter embedding  $z^{(p_j)}$  is concatenated with the output spatial features before they are processed by the feature decoder.

# **D** Qualitative Results

In the main paper, we demonstrated the rendered images of the Nyx test dataset. In this section, we provide additional qualitative results for the MPAS-Ocean and CloverLeaf3D datasets. All images were rendered using ParaView [2], an open-source platform built on the Visualization Toolkit (VTK) libraries.

#### D.1 MPAS-Ocean

Each instance in the MPAS-Ocean ensemble dataset comprises 60 depth levels. For visualization, we selected six layers from a single test instance, presented in Figure 6. We can observe that layers closer to the sea surface, such as layer 1 and layer 10, generally exhibit higher temperatures and contain more complex features.

Moreover, we compare the rendering results of our method with other baseline approaches as demonstrated in Figure 7 and Figure 8. A difference map is provided alongside each zoomed-in visualization to highlight prediction errors.

#### D.2 CloverLeaf3D

The visual comparisons between FA-INR and other baseline approaches are presented in Figure 9 and Figure 10, using two representative test instances from the CloverLeaf3D dataset. Compared to the MPAS-Ocean results, larger visual differences are observed across all methods on this more challenging dataset. Both FA-INR and Neural Experts achieve top accuracy on these two cases. A possible explanation is that both methods utilize the Mixture-of-Experts (MoE) framework, which enables them to effectively handle the complex and high-variation patterns present in CloverLeaf3D.

# **E** Gating Module in FA-INR

As introduced in subsection 4.2, the gating module contains a low-resolution feature grid and a linear projection layer. In our main experiments, we fixed the feature grid resolution at 16<sup>3</sup> across all three datasets, since using a small feature grid offers more efficient and stable optimization compared to other alternatives such as MLP, especially at the early training stage.

In this section, we investigate how varying the resolution of the feature grid impacts overall model performance. As shown in Table 5, a low-resolution grid  $(16^3)$  is sufficient to achieve high fidelity. Increasing the grid resolution does not necessarily lead to performance improvement, while the number of model parameters substantially increases. This observation is consistent with findings from previous studies [3, 11].

Metric	$16^{3}$	$32^{3}$	$64^{3}$
#Params	1.10M	1.56M	5.23M
#Experts	10	10	10
PSNR↑	51.92	51.59	52.66
$MD\downarrow$	0.1536	0.1561	0.1605

Table 5: Experimental results of varying feature grid resolutions in the gating module on the MPAS-Ocean dataset.

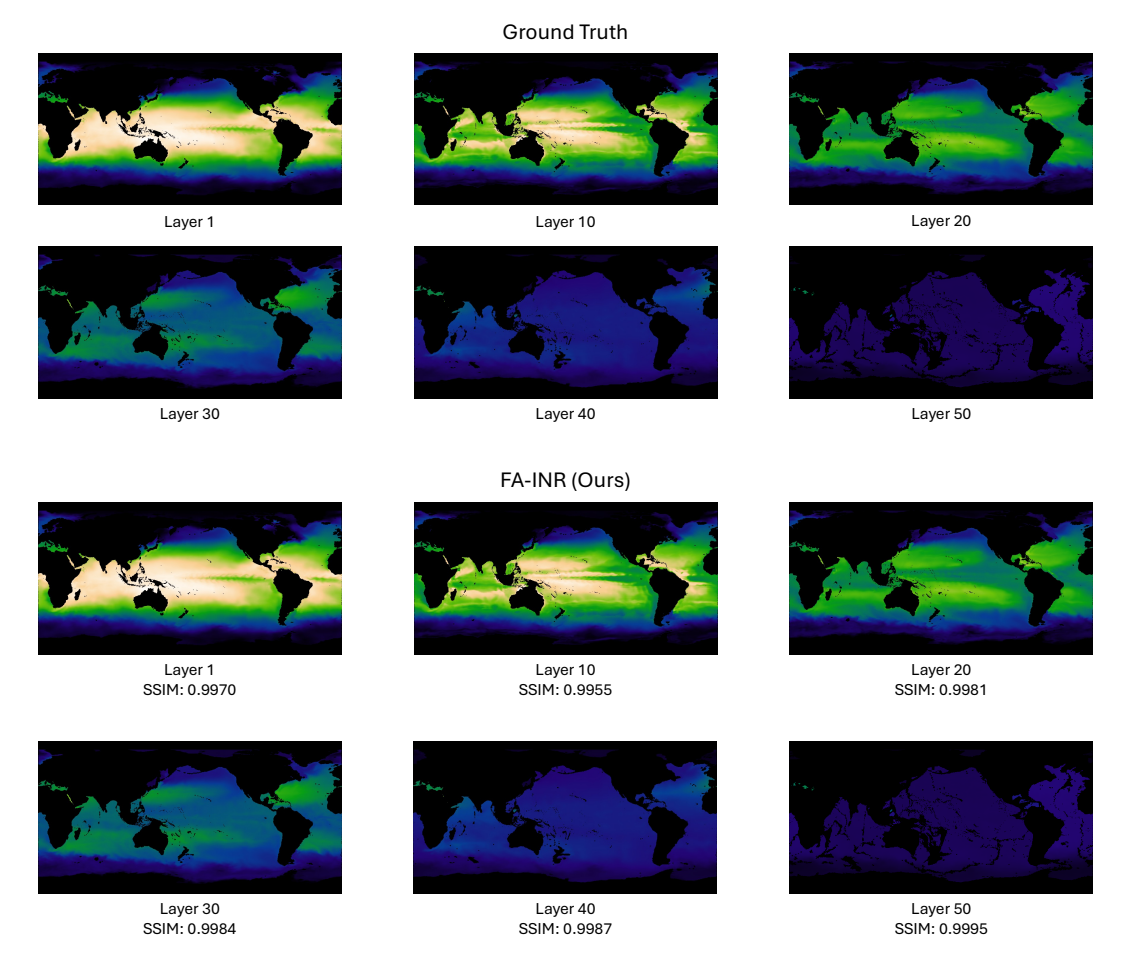


Figure 6: We select one test ensemble member from the MPAS-Ocean dataset, where each member contains 60 depth layers. In the visualizations, lighter colors indicate higher temperatures. Our proposed FA-INR consistently produces high-quality predictions across all depth levels.

## F Alternative Approach for Expert Aggregation

The proposed FA-INR utilizes a Mixture of Experts (MoE) architecture with Top-2 routing strategy, effectively balancing training efficiency and prediction accuracy. This section discusses two alternative expert arrangement strategies.

First, instead of making the Top-2 selection, one alternative forwards each input to all expert encoders simultaneously. The outputs from all experts are concatenated into a single large feature vector, which is then projected back to the original feature dimension before being processed by the feature decoder. As presented in Table 6, the original MoE design with Top-2 expert selection outperforms this concatenation strategy, particularly achieving a 34% improvement in the MD metric. We hypothesize that the performance degradation arises because, unlike the MoE framework where experts can develop specialized knowledge, the concatenation method forces every expert to process all inputs. This can lead to duplicated representations across experts, substantially increasing training time while limiting prediction accuracy.

Second, we evaluated a *weighted sum* strategy over all experts, where the outputs from all experts are aggregated using learned weights instead of sparse gating. Although this approach provided a slight improvement in overall accuracy compared to Top-2 routing, as shown in Table 6, it substantially increased inference time. Specifically, on a single A100 GPU, the Top-2 routing strategy required only 1.70 seconds per test field, whereas the weighted sum strategy took 7.42 seconds. These

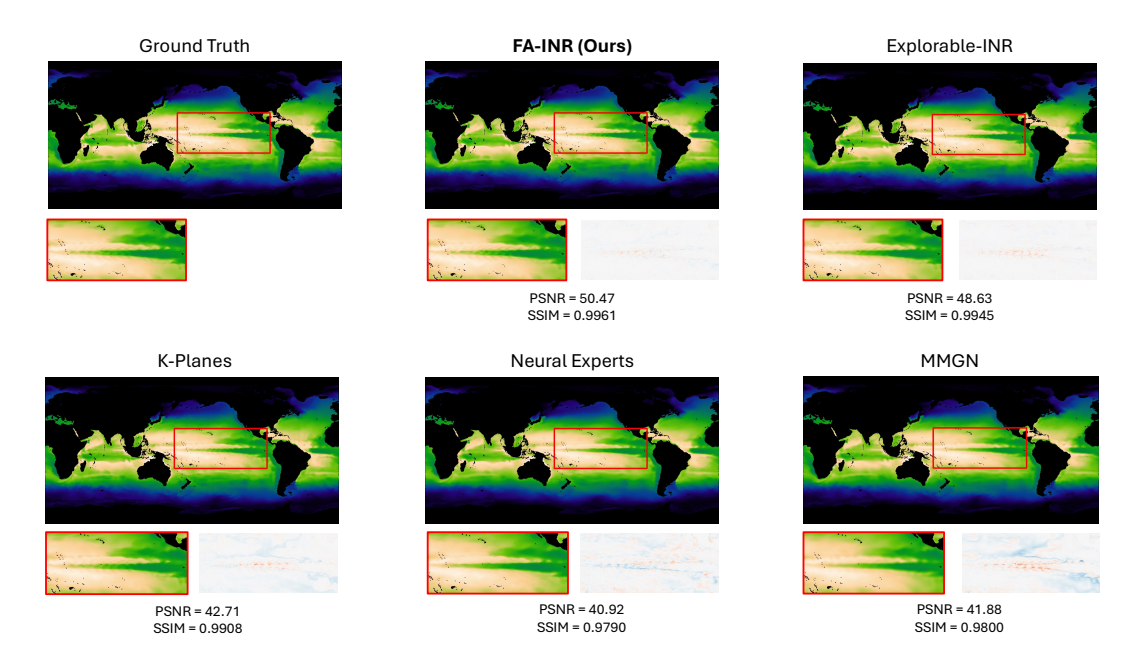


Figure 7: We select a layer close to the sea surface, which exhibits rich and high-variation features. Prediction errors are highlighted in the small figures on the right. The zoomed-in results reveal that the Neural Experts and MMGN struggle with modeling the high-frequency details.

results highlight that activating more experts per spatial input significantly increases computational overhead. Therefore, our sparsely-gated Top-2 routing approach offers a more practical balance between computational efficiency and model accuracy.

Metric	MoE	Concatenation	Weighted Sum
#Experts	10	10	10
PSNR↑	51.92	50.75	53.51
$\mathrm{MD}\!\!\downarrow$	0.1536	0.2061	0.1421

Table 6: Comparison of encoder expert utilization strategies (*i.e.*, Top-2 selection *vs.* all-expert concatenation *vs.* weighted sum over all experts) on the MPAS-Ocean dataset.

# **G** Generalization in Spatial Domain

While our proposed FA-INR surrogate is primarily designed to improve generalization across **unseen simulation parameters** (as demonstrated in subsection 5.2), we further evaluate its ability to generalize to **unseen spatial locations**. This evaluation provides complementary insight under a different generalization setting.

Specifically, during training, we randomly select 70% of the spatial coordinates within each of the 70 ensemble members and reserve the remaining 30% as a test set. This setting keeps the simulation parameters fixed and only evaluates generalization over spatial locations.

The quantitative results across all baselines are summarized in Table 7. Overall, FA-INR consistently outperforms baseline INR models, achieving an average improvement of 13.67% in PSNR and 42.59% in MD. Interestingly, Explorable-INR exhibits relatively poor spatial generalization compared to its performance in the main experiments. In contrast, K-Planes achieves competitive performance on both metrics, indicating that although K-Planes shows difficulty in generalization across simulation parameters, its multi-resolution feature planes are particularly effective for modeling spatial variations. However, this comes at the cost of significantly more model parameters.

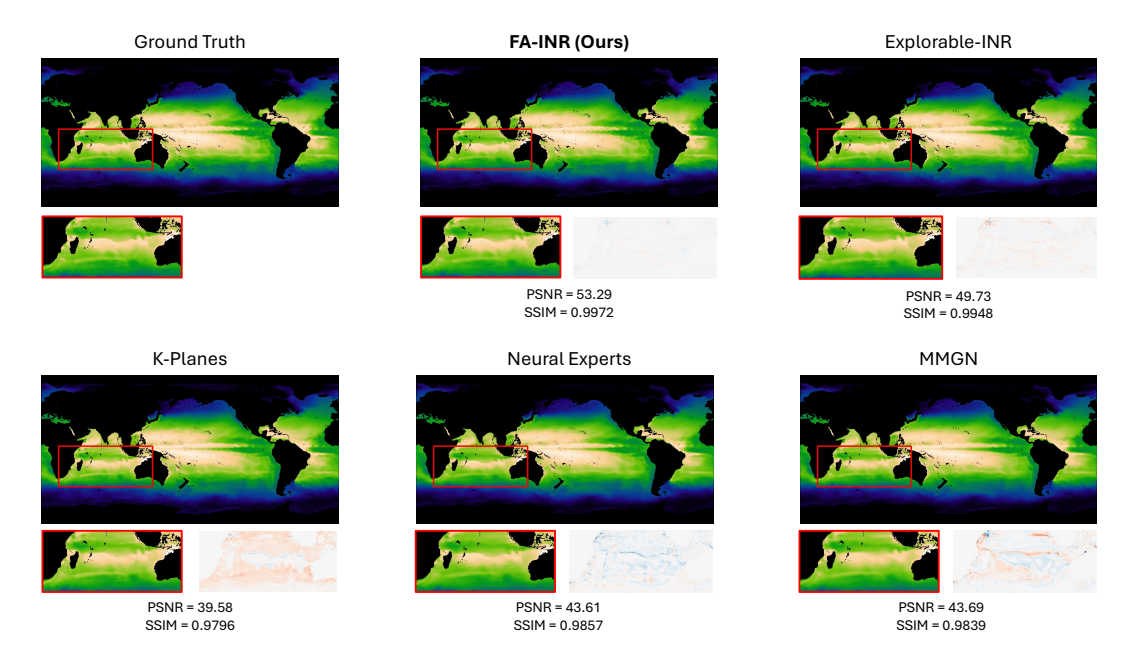


Figure 8: We select the same layer as in Figure 7 but from a different ensemble instance. Our proposed FA-INR achieves the highest prediction accuracy compared to the baseline approaches.

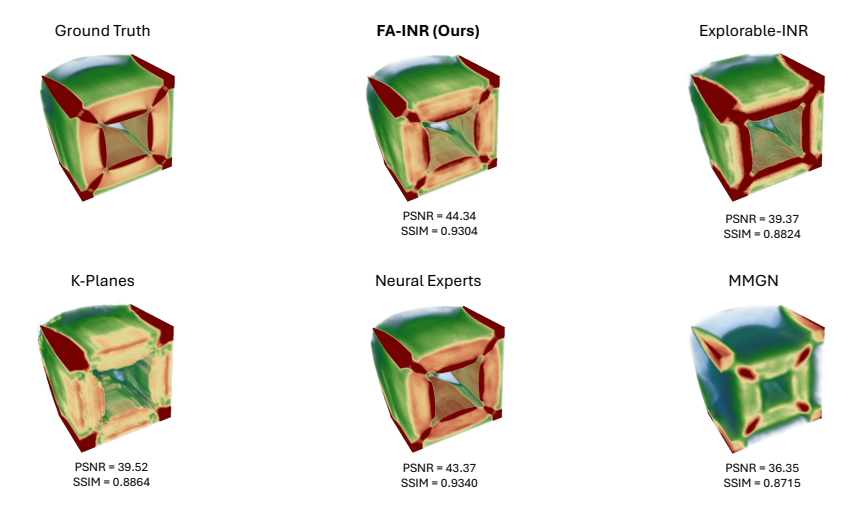


Figure 9: A representative test case from the CloverLeaf3D dataset is shown. Significant visual differences can be observed across the rendering results from all methods. Both FA-INR and Neural Experts, which utilize the MoE architecture, achieve the top prediction accuracy.

## **H** Discussion and Limitations

We propose Feature-Adaptive INR (FA-INR), a compact, embedding-augmented implicit neural representation designed for high-fidelity surrogate modeling of scientific ensemble simulations. Beyond its technical contributions, our approach also enables more interpretable predictions by allowing analysis of which model components contribute to outputs at specific spatial locations. This can be achieved by identifying the selected encoder experts and the most highly activated key-value pairs. Enhancing model transparency and reliability is particularly important for scientific research applications.

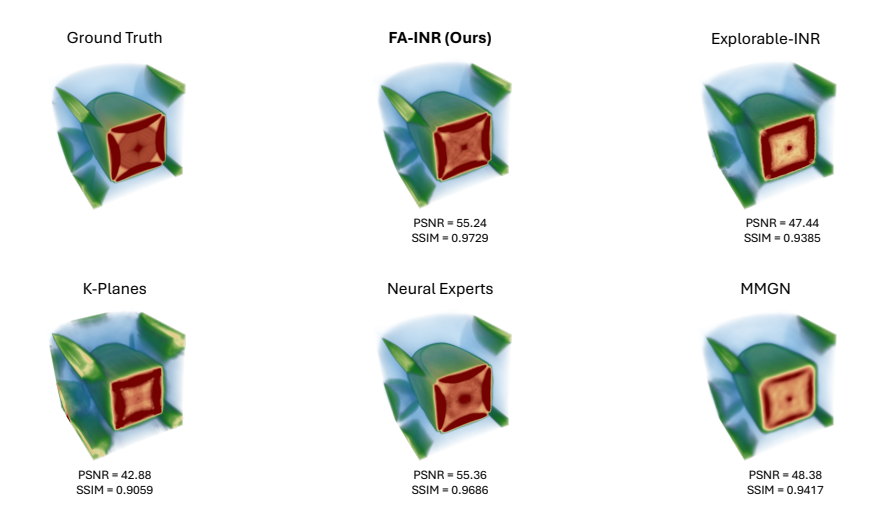


Figure 10: Another representative test case from the CloverLeaf3D dataset. Both FA-INR and Neural Experts, which utilize the MoE architecture, achieve the top prediction accuracy.

Metric	FA-INR (Ours)	Explorable-INR	K-Planes	Neural Experts	MMGN
#Params	1.10M	7.38M	43.17M	1.10M	1.10M
#Experts	10	-	-	10	-
PSNR↑	52.20	49.89	51.04	40.28	44.17
$MD\downarrow$	0.1657	0.3918	0.1665	0.4135	0.3471

Table 7: Evaluation of generalization to **unseen spatial locations** on the MPAS-Ocean dataset. Note that this spatial generalization task is distinct from the task in our main paper, which focuses on generalization across unseen simulation parameters.

We identify several directions for future work. First, we aim to expand our evaluation to include more ensemble datasets. However, our current setup, which covers three datasets from diverse scientific domains, already represents one of the most comprehensive evaluations compared to existing work on scientific data [9, 25]. Second, a limitation of our FA-INR is that our model requires slightly longer training time compared to the previous INR models using explicit representations, such as grids or planes. This is mainly because our method relies on cross-attention mechanism unlike the previous methods which support direct spatial indexing. Moreover, the use of a Mixture-of-Experts (MoE) architecture further introduces additional training time. However, considering the substantial time saved from running a numerical simulator and the improvements we achieve in surrogate modeling, this additional training time can be considered negligible.